Since January 2020 Elsevier has created a COVID-19 resource centre with free information in English and Mandarin on the novel coronavirus COVID-19. The COVID-19 resource centre is hosted on Elsevier Connect, the company's public news and information website.

Journal of Molecular Structure 1243 (2021) 130705

Contents lists available at ScienceDirect

Journal of Molecular Structure

journal homepage: www.elsevier.com/locate/molstr

Chemical reactivities and molecular docking studies of parthenolide with the main protease of HEP-G2 and SARS-CoV-2

Abdelhak Ouled Aitouna[a], ME. Belghiti[b,g,*], Aslı Eşme[c], E. Anouar[d], Anass Ouled Aitouna[e,f], A. Zeroual[e,*], M. Salah[e], A. Chekroun[a], H. El Alaoui El Abdallaoui[e], A. Benharref[a], N. Mazoir[f,g]

[a] Laboratory of Biomolecular Chemistry, Natural Substances and Reactivity, URAC 16, Faculty of Sciences Semlalia, Cadi Ayyad University, P.O. Box 2390, Marrakech, Morocco
[b] Laboratory of Nernest Technology, 163 Willington Street, Sherbrook, QC J1H5C7, Canada
[c] Department of Elementary Science Education Faculty of Education Kocaeli University, Umuttepe, Kocaeli 41380, Turkey
[d] Chemistry Department, College of Sciences and Humanities, Prince Sattam bin Abdulaziz University, P.O. Box 83, Al Kharj 11942, Saudi Arabia
[e] Molecular Modelling and Spectroscopy Research Team, Faculty of Science, Chouaïb Doukkali University, P.O. Box 20, El Jadida 24000, Morocco
[f] Laboratory of Plant Biotechnology and Ecosystem Valorization (LB2VE), Research Unit: Natural Resource Valorizations, Faculty of Sciences Chouaib Doukkali University, P.O. Box, El Jadida 24000, Morocco
[g] Department of Chemistry, Chouaib Doukkali University, P.O. Box El Jadida 24000, Morocco

ARTICLE INFO

Article history:
Received 2 April 2021
Revised 30 April 2021
Accepted 12 May 2021
Available online 19 May 2021

Keywords:
Epoxidation
ELF
Docking calculation
DFT
Parthenolide
SARS-CoV-2

ABSTRACT

We have used bioinformatics to identify drugs for the treatment of COVID-19, using drugs already being tested for the treatment as benchmarks like Remdesivir and Chloroquine. Our findings provide further support for drugs that are already being explored as therapeutic agents for the treatment of COVID-19 and identify promising new targets that merit further investigation. In addition, the epoxidation of Parthenolide **1** using peracids, has been scrutinized within the MEDT at the B3LYP/6–311(d,p) computational level. DFT results showed a high chemoselectivity on the double bond C_3=C_4, in full agreement with the experimental outcomes. ELF analysis demonstrated that epoxidation reaction took place through a one-step mechanism, in which the formation of the two new C-O single bonds is somewhat asynchronous.

1. Introduction

Epoxidation is a reaction of both industrial and academic importance [1]. The formed epoxides [2–6] represent an extremely useful intermediate which could be converted to higher value chemical compounds [7]. Moreover, epoxides are present in a large range of natural products [8,9] and biologically active compounds [10–13]. Epoxides can be accessed in numerous ways, but the most common method consist the epoxidation of olefins using peracids [14]. Peracids are widely used for the epoxidation of olefins; owing to their high reactivity permit them to be used under relatively mild reaction conditions without using any catalyst, the m-CPBA being the most widely used in epoxidation (Scheme 1).

The interest for the use of oxidizing agents which are safe for the environment keeps increasing. Indeed, hydrogen peroxide (H_2O_2) is a very interesting alternative since its secondary decomposition products are water and oxygen. It is less expensive and more accessible than some of the traditional oxidizing agents. Consequently, from both ecological and economical decision, it is enviable to utilize a catalytic epoxidation employing aqueous hydrogen peroxide as oxidant, and transition metal complexe as catalysis. The substrate employed such as transition metal complexes became very attractive technologies and environmentally friendly asymmetric epoxidation. The current reports have described several remarkable catalytic systems in the presence of hydrogen peroxide such as iron [15], tungsten [16], vanadium [17,18], Manganese [19–21], bicarbonate [22,23] and dioxolane [24]. Various theories have been developed to elucidate the molecular mechanism, reactivity and selectivities (regio, chemo and stereo). The bonding evolution theory (BET) [25], the conceptual density functional theory (CDFT) [26], and the electron localization function (ELF) method [27], have presented to scrutinize the reaction mechanism [28] within a current model named a molecular electron density theory (MEDT) [29]. Our theoretical studies devoted to the

* Corresponding authors.
E-mail addresses: elbelghiti10@gmail.com (ME. Belghiti), zeroualabdellah2@gmail.com (A. Zeroual).

https://doi.org/10.1016/j.molstruc.2021.130705
0022-2860/

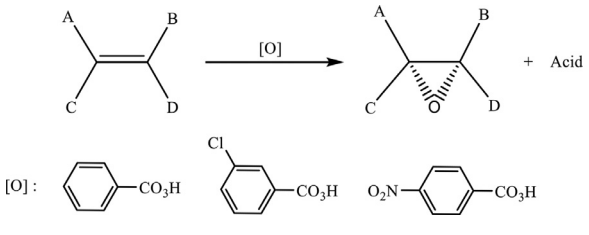

Scheme 1. Epoxidation of olefins using peracids.

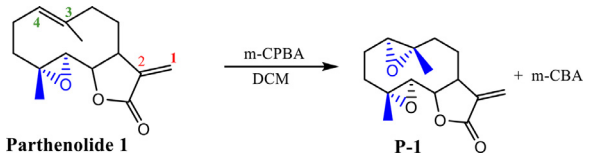

Scheme 2. Epoxidation of the starting materials **1.**

epoxidation of R-carvone with peracid demonstrate a high chemoselectivity involving the $C = C$ double bond carrying the methyl group and the low diastereoselectivity [30].

The many medicinal properties of parthenolides products we have tried to investigate about its efficiency against cancer and SARS-CoV-2 by docking protocol, seen that the novo development of antivirals in vitro need a very long time-, expensive cost-, and effort-intensive endeavor.

New double mutant variant discovered in India continues to spread around the world, with specialists more than once stressing the importance of changing our way of life in order to stay safe [31–34]. Thus, in this moment, it is important to generate specific antivirals especially for SARS-CoV-2 [35–38] in very short time by testing potential medicinal compounds in silico, seen the increasing structural data of key proteins [39,40].

Molecular docking provides a powerful tool in understanding the degree of recognition between the tested compounds and the amino acids of the enzyme active site. Throughout the virtual screening, the ligand molecules were flexible and macromolecule was kept as rigid [33].

In this context, we have examined influence of parthenolides products **(4–7)** against Coronavirus (Covid-19) using Docking tools and we have also studied the stereoisomerism (parthenolides **2, 3**) against cancer (Fig. 1), after a MEDT study toward the epoxidation reaction of parthenolide **1** in order to comprehend the formation of epoxide compound plus the chemoselectivity (Scheme 2) [41],

2. Computational methods

DFT computations were executed employing the B3LYP functional [42,43] jointly with the 6–311G(d,p) basis set [44]. Optimizations were supported out utilizing the Berny analytical gradient optimization technique [45,46]. The stationary points were described by frequency calculations so as to confirm that TSs have only one imaginary frequency. The intrinsic reaction coordinates [47] (IRC) paths were drawn to pattern the energy profiles joining every TS to the two related minima [48,49]. The impact of dichloromethane (DCM) as solvent was considered by full improvement of the gas stage structures utilizing the polarisable continuum model (PCM) developed by Tomasi's group [50–53]. Conceptual DFT (CDFT) global reactivity indices [54] and Parr functions were calculated exploiting the equations contributed in reference [55]. Each calculation was carried out with the Gaussian 09 [56]. Topological analyses of the ELF were functioned with the TopMod package using the monodeterminantal wave functions [57].

Table 1
B3LYP/6–31G(d) electronic chemical potential μ, chemical hardness η, electrophilicity ω, nucleophilicity N, in eV, of compounds **1**, ethaneperoxoic acid (EPA) **2**, and m-chloroperbenzoic acid (m-CPBA) **3**.

System	H	μ	Ω	N
1	4.86	−3.86	1.53	3.22
2	7.39	−4.00	1.08	1.83
3	5.41	−4.36	1.76	2.45

3. Results and discussion

3.1. Analysis of the CDFT indices of the reagents

Numerous studies devoted to organic reactions have shown that the examination of the reactivity indices defined within CDFT [58] is a powerful tool to understand organic chemical reactivity. Thus, in order to predict the reactivity of parthenolide **1** in epoxidation reaction, the global indices gathered in Table 1, i.e. the electronic chemical potential, μ, chemical hardness, η, electrophilicity, ω, and nucleophilicity, N, are analyzed.

The electrophilicity ω indices of the alkene **1** and 1.53 eV whereas the nucleophilicity N indices are 3.22 eV, respectively, these values allow classifying alkene **1** as strong electrophiles and strong nucleophiles within the electrophilicity and the nucleophilicity scales [59]. The electrophilicity ω indices of the oxidants **EPA** and **m-CPBA** are 1.08 and 1.76 eV, while the nucleophilicity N indices are 1.83 and 2.45 eV, respectively. Thus, the oxidant EPA is classified as a moderate electrophile and a marginal nucleophile, while m-CPBA is classified as a strong electrophile and a moderate nucleophile. In this epoxidation the alkene **1** will participates as nucleophiles and the oxidants **EPA** and **m-CPBA** as electrophiles.

In recent times, the electrophilic P_k^+ and nucleophilic P_k^- Parr functions have been proposed to examine the local reactivity involving reactions between a nucleophile/electrophile pair [60,61]. Therefore, the nucleophilic P_k^- Parr functions for parthenolide **1** are analyzed (Fig. 2).

Examination of the nucleophilic P_k^- Parr functions of parthenolide **1** shows that the carbons of the double bond C_3=C_4 ($P_3^- = 0.39$ and $P_4^- = 0.25$) are the most nucleophilic centers of this molecule, note that C_3=C_4 double bond is multiple more nucleophilically activated than the exocyclic double bond C_1=C_2 ($P_1^- = 0.007$ and $P_2^- = 0.006$). This prediction is in good agreement with the experimental results.

3.2. Energetic study of epoxidation

3.2.1. Energetic study of the epoxidationof parthenolide1 by EPA and m-CPBA

Owed to the non-symmetry of parthenolide **1** and peracids (**2** and **3**), two competitive reaction channels are feasible for the reaction between them. There are related to the two regioisomeric approach modes of the parthenolide relative to the double bond C_3=C_4 and double bond C_1=C_2. The investigation of the stationary points elaborates in the epoxidation of parthenolide **1** and peracids **2** and **3** shows that these reactions follow a one-step mechanism. Therefore, the reactions between parthenolide **1** and peracid followed by the two TSs for each peracid represented by **TS-1, TS-2, TS-3**, and **TS-4** and their corresponding epoxides, Relative energies are arranged in Scheme 3 and complete energies data are showed in Tables S1. The Gibbs free energies profiles of the reaction paths associated with the epoxidation reaction of parthenolide **1** and peracid are presented in Fig. 3, while the complete thermodynamic data are given in Table S2 in Supplementary Material.

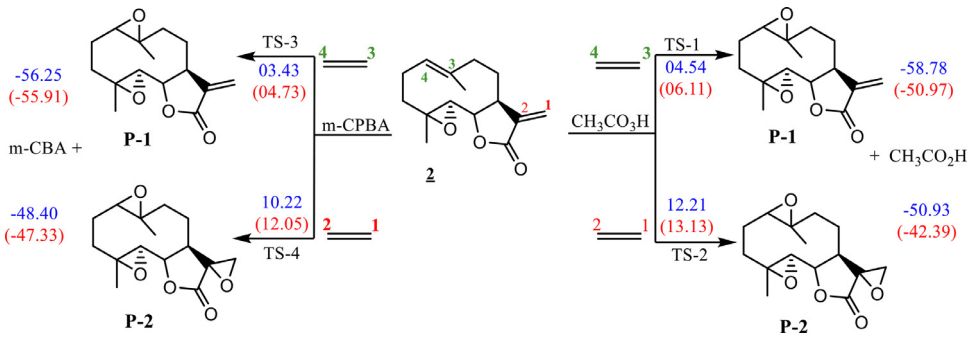

Scheme 3. The considered regioisomeric reaction paths associated to the epoxidation of parthenolide **1** using m-CPBA and CH_3CO_3H.

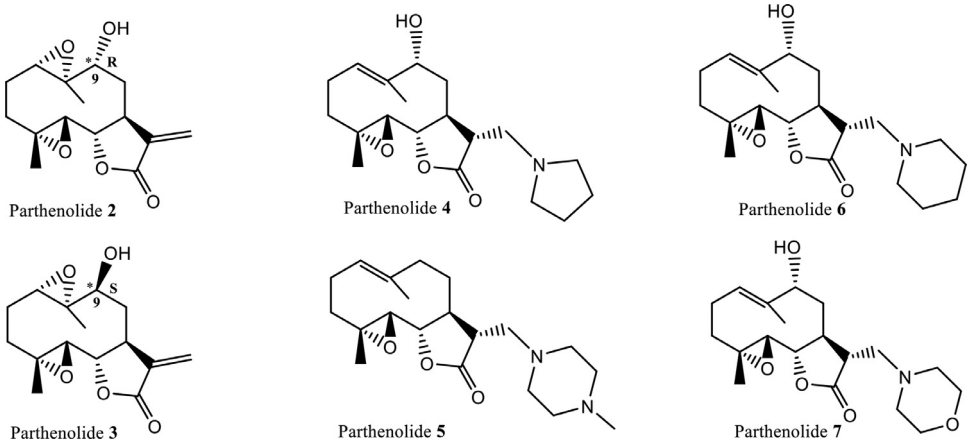

Fig. 1. Parthenolide products **2** and **3** tested against cancer and parthenolide products (**4**–**7**) tested against coronavirus (COVID-19).

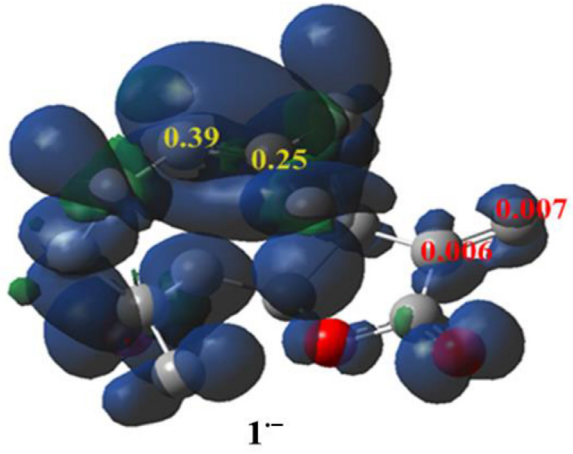

Fig. 2. Three-dimensional (3D) representations of the Mulliken atomic spin densities of radical anion together with the nucleophilic P_k^- Parr functions of compound **1**.

The gas phase activation energies associated with the competitive reactive channels are found in the narrow range of 3.4–12.4 kcal mol^{-1}. These epoxidation reactions are strongly exothermic, between 42 and 59 kcal mol^{-1}. Analysis of these relative energies leads to various attractive conclusions: (1) this epoxidation reaction presents very low activation energy, evidencing the high reactivity of parthenolide **1** with m-CPBA (or CH_3CO_3H); (2) this epoxidation reaction is a very high regioselectivity, as the most favourable TS-1 (TS-3) is 7.67 kcal mol^{-1} (6.79 kcal mol^{-1}) higher in energy than TS-2 (TS-4); (3) the strong exothermic character of this epoxidation reaction makes the formation of epoxides P-1 and P-2 irreversible. Consequently, the formation of the epoxide P-1 is under kinetic and thermodynamic control.

In DCM, the activation energies associated with the two competitive reactive channels are found in the narrow range of 4.7–13.2 kcal mol^{-1}, these epoxidation reactions being strongly exothermic by ca.42–56 kcal mol^{-1}. Examination of these relative energies conduct to two interesting conclusions: (1) addition of solvent effects does not create significant change neither in the kinetics nor in the thermodynamics of the reaction; and (2) while the selectivity slightly increases as TS-1is 7.02 kcal/mol higher in energy than TS-2 and solvent effects markedly increase the regioselectivity as when we use m-CPBA as oxidantTS-3 is 7.32 kcal mol^{-1} higher in energy than TS-4, in equitable agreement with the experimental results [39].

The Gibbs free energies profiles of the reaction paths associated with the epoxidation of parthenolide 1 by m-CPBA and CH_3CO_3H are presented in Fig. 3.

Adding the thermal corrections to the total electronic energies does not substantially modify the relative enthalpies when parthenolide **1** has been oxidized by m-chloroperoxybenzoic acid. While the relative enthalpies decrease by 1,2 kcal mol^{-1}, the exothermic character of the reaction decreases by 3,4 kcal mol^{-1}. These unappreciable changes do not modify the chemoselectivity found by analysis of the electronic energies. The addition of the entropy contribution to the enthalpies increases the relative Gibbs free energies between 11 and 12 kcal mol^{-1} as a consequence of the unfavorable entropies associated with these bimolecular processes, between 40 and 45 cal mol^{-1} K^{-1}. As a consequence, the activation Gibbs free energy associated with the most favourable *endo* reactive channel rises to 17.50 kcal mol^{-1}. This channel being exergonic by 52.28 kcal mol^{-1}, considering the relative Gibbs free energies of the two competitive TSs, while the *endo* chemoselectivity decreases slightly by 0.69 kcal mol^{-1}. The gas phase geometries

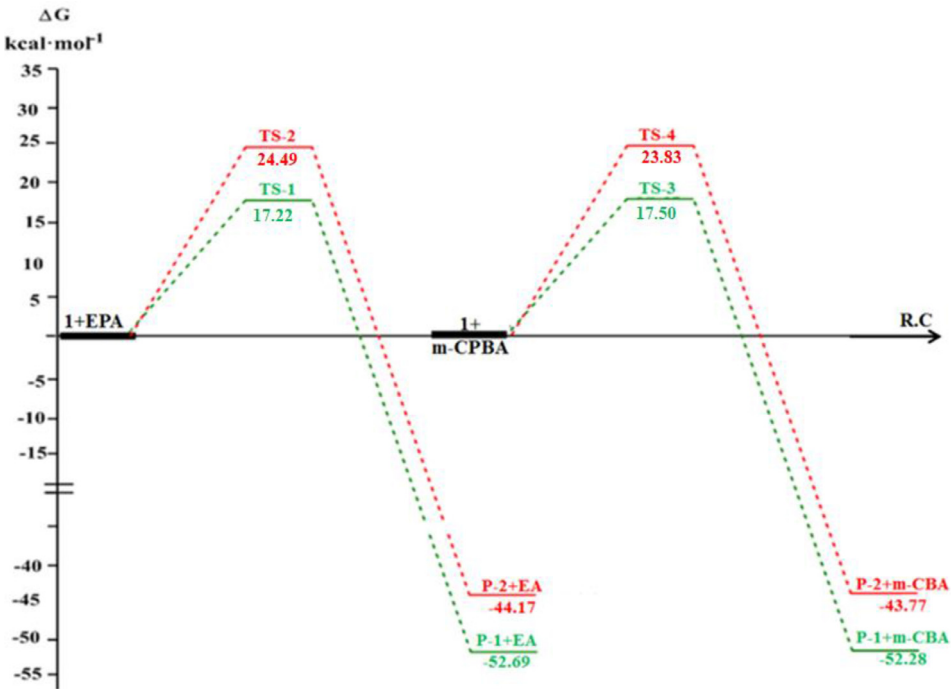

Fig. 3. Gibbs free energy (ΔG) profiles in kcal•mol^{-1}, for the studied reaction paths of the epoxidation of compound **1**using m-CPBA and CH_3CO_3H, in the presence of dichloromethane (DCM) at 25°C.

of the TSs involved in the competitive reaction channels are given in Fig. 4. At the **TS-1** and **TS-3**, the lengths of the O–C3 and O–C4 forming bonds are 1.998 and 2.105 Å (**TS-1**) and 2.052 and 2.271 Å (**TS-3**), while at the *exo* TSs, the lengths of the O–C1 and O–C2 forming bonds are 2.193 and 1.886 Å (**TS-2**) and 2.193 and 1.884 Å (**TS-4**). Some appealing conclusions can be drawn from these geometrical parameters: (1) the TSs associated with the channels are more asynchronous than those associated with the *exo* ones; and (2) at the TSs associated with the *endo* channels, the O–C3 bond formation involving the epoxide **P-1** is more advanced than the O-C4 one.

3.2.2. Comparative study between epoxidation of parthenolide1 by m-CPBA and CH_3CO_3H

According to transition state theory (TST), the second order rate constant (k_{TST}) at a given temperature (T) can be determined using the following equation [62,63]:

$$\mathbf{K_{TST} = \frac{k_B T}{hC_0} e^{\frac{-\Delta G^{\#}}{RT}}}$$

Where k_B, h, C_0, and R denote Boltzmann's constant, Planck's constant, standard concentration (1 mol l^{-1}), and the universal gas constant R = 1987 cal•K^{-1}•mol^{-1}, respectively.

It is considered that K_{TST}(ETPA), the rate constant of the epoxidation reaction of parthenolide **1** by CH_3CO_3H and K_{TST}(m-CPBA), the rate constant epoxidation reaction of **1** using m-CPBA:

$$\mathbf{K_{TST}(ETPA) = \frac{k_B T}{hC_0} e^{\frac{-\Delta G^{\#}(ETPA)}{RT}}}$$

$$\mathbf{K_{TST}(m-CPBA) = \frac{k_B T}{hC_0} e^{\frac{-\Delta G^{\#}(m-CPBA)}{RT}}}$$

$$\mathbf{\frac{K_{TST}(ETPA)}{K_{TST}(m-CPBA)} = \frac{\frac{k_B T}{hC_0} e^{\frac{-\Delta G^{\#}(ETPA)}{RT}}}{\frac{k_B T}{hC_0} e^{\frac{-\Delta G^{\#}(m-CPBA)}{RT}}} = e^{\frac{\Delta G^{\#}(m-CPBA) - \Delta G^{\#}(ETPA)}{RT}}}$$

$$\mathbf{K_{TST}(ETPA) = 1.6 * K_{TST}(m-CPBA)}$$

This result indicates that the epoxidation reaction rate using ETPA is greater than the epoxidation rate by m-CPBA, which shows that the use of CH_3CO_3H is more effective than m-CPBA and also an environmentally friendly oxidant for which ethanoic (or acetic) acid is the sole byproduct.

3.3. ELF topological analysis of the C-O bond creation along the epoxidation reaction of parthenolide 2 by ethaneperoxoic acid

So as to describe the C-O bond creation in the epoxidation reaction of parthenolide **1** by ethaneperoxoic acid, a topological investigation of the ELF along the IRC related with the favourable reaction path was executed. The IRC structures precisely implicated in the formation of the new C–O single bonds were chosen by accomplishing the topological analysis of the ELF for all the structures of the IRC having $2.6 > d(O - C) > 1.4$. The complete ELF analysis is displayed in ESI, while the attractor positions of the ELF basins are presented in Fig. 3S and ELF localization domains of the structures TS-1, VI, VII and *X* are donated Fig. 5. Numerous attractive conclusions can be tired from this ELF topological analyze: (i) the activation energy (TS-1 = 17.22 Kcal / mol) allows the O-O bond of the peracid to be disrupted, which is involved in the formation of the electronic density on the oxygen; (ii) topological analysis of the ELF of the TS-1 (I) indicates that the formation of the new O-C single bonds has not started yet, the only discrepancy is found in the O1-C4 region and we can note too that the bond O1-H is not yet dissociate; (iii) construction of the primary O-C single bond takes position at a O-C distance of ca. 1.92 Å, including an initial population of 1.19e, by distributing part of the non-bonding electron density of the C pseudoradical center; (iv) formation of the another O-C single bond takes place at a C-O distance of ca. 1.65 Å, with an primary population of 0.81e, by donating some O oxygen nonbonding electron density to the C2 carbon (Fig. 3S); and at end (v) taking into description the IRC values of the structures at which creation of the two single bonds occurs, i.e. ***X***, the bond formation can be considered asynchronous. The creation of another O-C single bond started after the formation of the first O-C single bond is

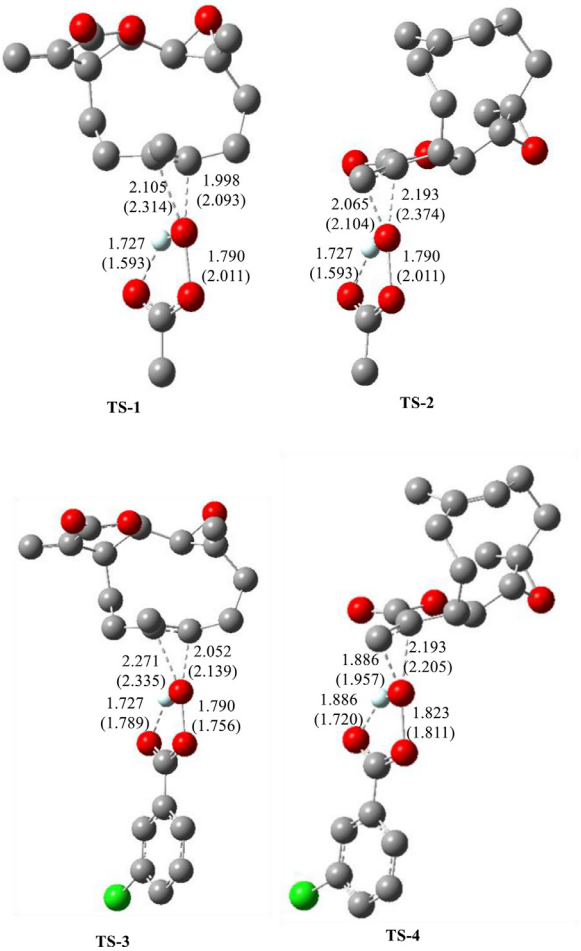

Fig. 4. B3LYP/6–311G(d,p) optimized geometries of the regioisomeric TSs involved in the epoxidation of compound **1** by m-CPBA. Values in DCM are given in parentheses. Distances are given in angstroms, Å.

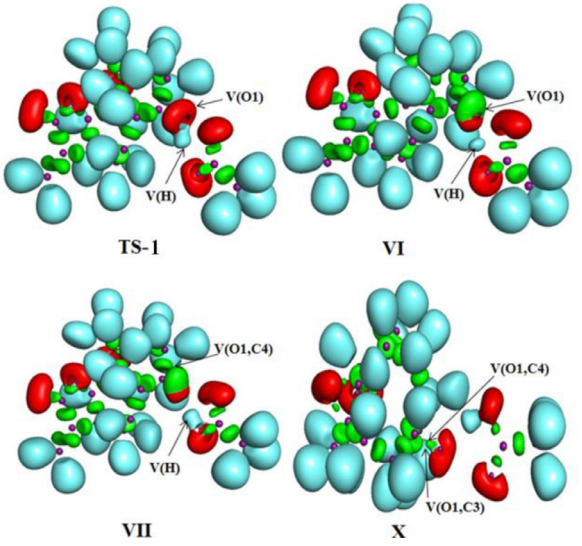

Fig. 5. B3LYP/6–311G(d,p) ELF localization domains of the structures TS-1, VI, VII and X involved in the formation of the two epoxide ring $C-O$ single bonds along the favourable reaction path associated with the epoxidation reaction of parthenolide **1** by peracetic acid, represented at an isosurface value of ELF = 0.75;.

completed via 100%. This conduct describes that this epoxidation reactions obtain place through a non-concerted *two-stage one-step* mechanism [70].

3.4. Hirshfeld surface analysis and molecular docking studies

3.4.1. Hirshfeld surface analysis

The most effective interaction between oxygen (O) and hydrogen (H) atoms can be seen as red areas in the Hirshfeld surface (HS) analysis, which provides a convenient analysis of intermolecular interactions within a crystal. The Hirshfeld surface is mapped using the normalized contact distance d_{norm}, defined in terms of d_i and d_e distances, which represent the distance from the Hirshfeld surface to the nearest nucleus inside and external the surface, respectively. All the Hirshfeld surfaces (d_{norm}, shape index, curvedness, and the related two-dimensional (2D) finger print plots) were performed by using the Crystal Explorer 3.1 [54]. H…H (48.3%) contacts summarized in the two-dimensional (2-D) fingerprint plot make the largest contribution to the Hirshfeld surfaces. As seen in Fig. 6. Hirshfeld, the O…H (44.1%) interactions occur as two distinct spikes in the upper right area of the 2-D fingerprint plots. The characteristic shape of C…H is similar to 'wings' as shown in Fig. 6. Hirshfeld and the percentage contribution of this contact is 7.0% for the studied compound.

3.4.2. Molecular docking studies against the HEP-G2 human liver cancer cell line

The parthenolide molecule and several structurally related analogs have recently been attributed to having anticancer properties [64,65]. Present study provides the influence of the stereoselectivity on anticancer activity for the parent parthenolides (9α-hydroxyparthenolide **2** and 9β-hydroxyparthenolide **3**). Molecular docking study was carried out to identify the potential binding affinities and the mode of interaction of the two parthenolides **2** and **3** against the HEP-G2 human liver cancer cell line (PDB: 3GCW) because the major application of parthenolide and its derivatives is as an anticancer agent. The minimum binding energies, inhibition constants and various parameters of the ligand-protein docking interactions were performed using the Autodock version 4.2 programs along with the graphical interface Auto Dock Tools 4 [66] and listed Table 2. Discovery Studio Visualizer software was used to analyze the output of docking process [67]. The 2D and 3D molecular surface maps of the most active compounds Parthenolide **2** and Parthenolide **3** docking into the 3GCW binding sites is shown in Fig. 7.

Parthenolide **3** showed conventional hydrogen bond and unfavorable Donor-Donor bond with amino acids TRP428 and ARG319 through the H atom of the hydroxy group, respectively, while Parthenolide **2** showed one conventional hydrogen bond with TRP428 amino acid through H atom of the hydroxy group (Fig. 7). Any unfavorable bond formation between the target protein-ligand complexes affects the activity stability of the drug since such bonds show a repulsive force between the protein and ligand. The residues TRP428, ARG319 interact well with the Parthenolide **2** and Parthenolide **3** showing the conventional bond length of 5.4, 1.8 and 4.7, 2.8 Å, respectively. The Parthenolide **2** and Parthenolide **3** when docked with the target protein 3GCW showed a binding affinity of −4.54 and −4.94 kcal/mol, respectively.

3.4.3. Molecular docking studies into the active site of the main protease of SARS-CoV-2

To test Parthenolide **4**-Parthenolide **7**, Remdesivir and Chloroquine compounds as probable targeted therapeutic agents of SARS-CoV-2, their molecular docking into the active site of the main protease (M^{pro}) of SARS-CoV-2: M^{pro} is investigated. The intermolecular interactions between of the tilted compounds and the active

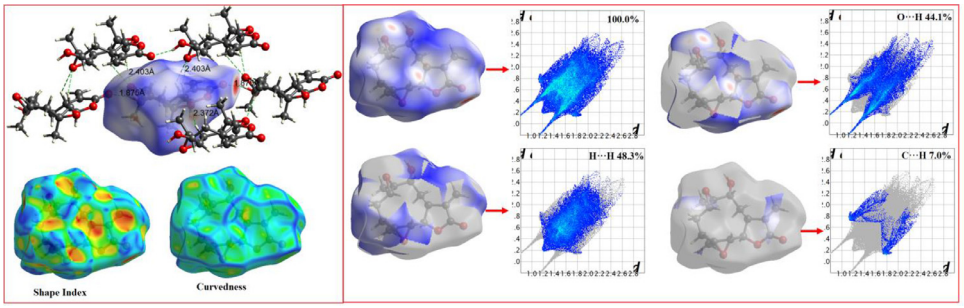

Fig. 6. D Hirshfeld surfaces (Shape index, Curvedness) and 2D- Finger print with d_{norm} surface view of 9b–hydroxy-1b,10a-epoxyparthenolide.

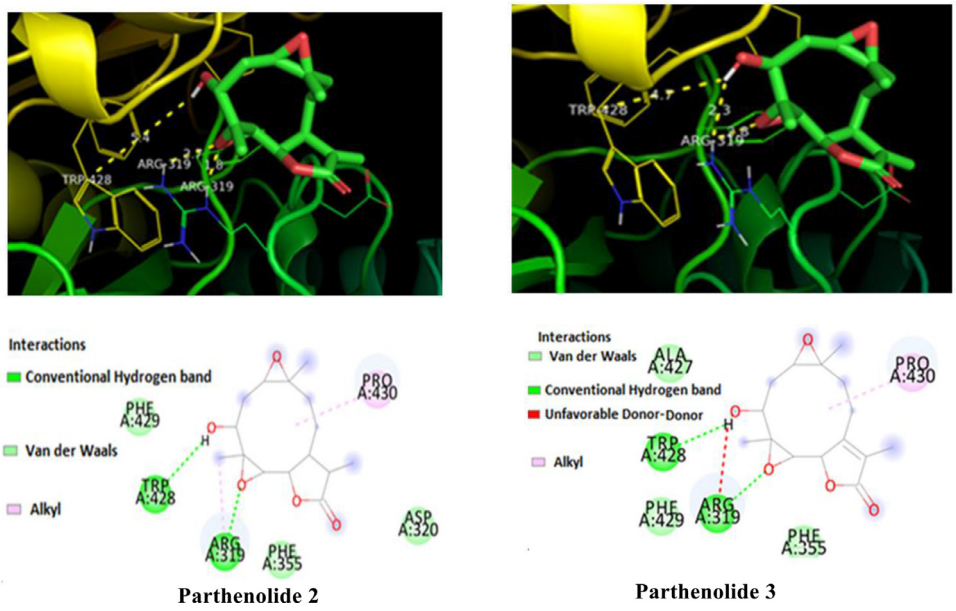

Fig. 7. The 3D and 2D interactions of Parthenolide **2** and Parthenolide **3** docked with the target protein 3GCW.

Table 2
The obtained docking parameters of parthenolides **2** and **3**.

Protein [PDB ID]	Bonded residues	Bond distances (Å)		Inhibition constant (μM)		Intermolecular energy (kcal/mol)		Binding energy (kcal/mol)		RMSD (Å)	
		2	**3**	**2**	**3**	**2**	**3**	**2**	**3**	**2**	**3**
3GCW	ARG319	1.8	2.3	469.74	239.24	−4.84	−5.24	−4.54	−4.94	11.04	11.29
	ARG319	2.7	2.8								
	TRP428	5.4	4.7								

residues of main protease have been explored using Auto dock package [66]. The staring geometries of main protease and the original docked ligand N3 were download from the RCSB data bank web site (PDB code 6LU7) [68]. The re-docking of the original ligand into the active site of main protease is relatively well reproduced with a RMSD value of 2 Å. Stepwise of molecular docking study is reported in our previous study [69]. The binding affinity of Parthenolide**4**-Parthenolide **7**, Remdesivir and Chloroquine compounds to active site of the main protease may strongly depend on the structural geometry of its basic skeletons, and the presence of specific substituted groups and heteroatoms (Fig. 8). In an attempt to determine the role of these parameters, molecular docking study has been carried out to determine their binding modes of Parthenolide **4**-Parthenolide **7**, Remdesivir and Chloroquine with main protease. Table 3 summarized the calculated binding energies of the stable complexes ligand-M^{Pro}, number of conventional intermolecular hydrogen bonding established between the docked compounds and the active site residues of main protease.

All the complexes formed between Parthenolide **4**, Parthenolide **7**, Remdesivir and Chloroquine compounds and the active residues of main protease display negative bending energies (Table 3), which may probably indicate their potency to act as SARS-CoV-2 therapeutic agents. The band energies of the stable complexes range −8.50 to −6.91 kcal. According to molecular docking results Parthenolide **5** showed highest affinity to the main protease with a binding energy of −8.50 kcalmol^{-1}. Parthenolide **4** and Parthenolide **7** differed by the substituted pyrrolidine, 1-methylpiperazine, piperidine and morphine groups at alpha position of dihydrofuranone ring (Fig. 1). The highest affinity of Parthenolide **5** is mainly referred to the presence of methylpiperazine. Indeed, the methylpiperazine formed three intermolecular carbon hydrogen bonds with amino acids GLU A166, LEU A167 and PRO A168 of distance 3.28, 3.00 and 3.58Å(Fig. 8). The Chloroquine showed the lowest binding energy with a binding energy of-8.91 kcal mol^{-1}. The low affinity may refer to the absence of strong intermolecular hydrogen bonding between the functional group of the

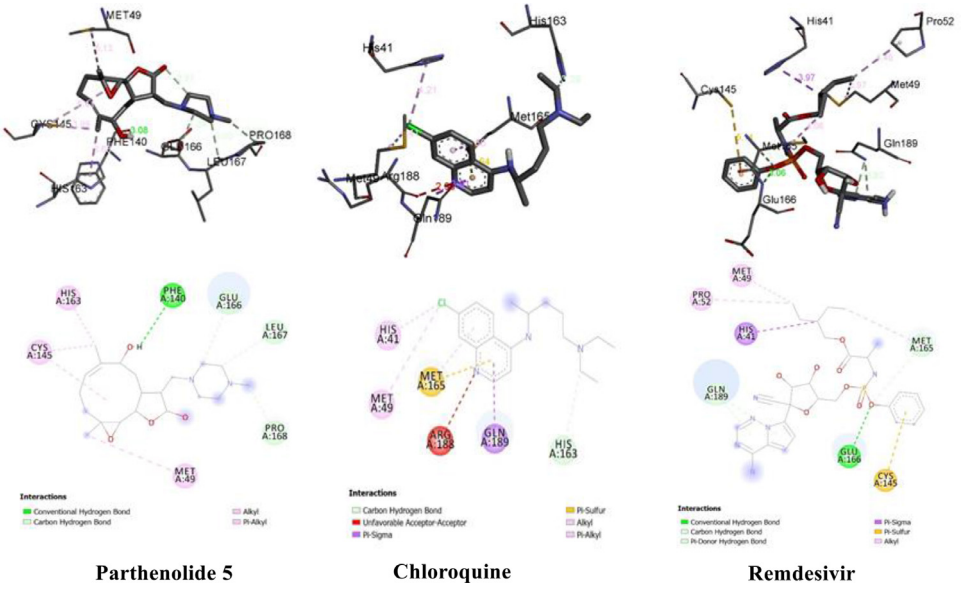

Fig. 8. 3D and 2D closest interactions between active site residues of main protease (M^{Pro}) and compounds Parthenolide **5**, Chloroquine and Remdesivir.

Table 3
Docking binding energies, conventional hydrogen bonding and the number of closest residues to the docked compounds into the active site of main protease.

Compound	Free binding energy (kcal/mol)	Conventional H-Bonds (HBs)	Number of closest residues to the docked ligand in the active site
Parthenolide **4**	−7.12	2	4
Parthenolide **5**	−8.50	1	7
Parthenolide **6**	−7.26	1	5
Parthenolide **7**	−7.02	0	5
Remdesivir	−7.99	1	7
Chloroquine	−6.91	0	5

Chloroquine and the amino acids of the main protease (Fig. 8). Remdesivir-M^{Pro} showed relatively comparable binding energy to the stable one Parthenolide **5**-MPro with a relative energy of 0.5 $kcalmol^{-1}$. In Remdesivir-M^{Pro}, a strong intermolecular hydrogen bond was formed between GLU A 166 and lone pair of oxygen atom for benzoate of 3.06 Å (Fig. 8).

The molecular docking results revealed that Remdesivir has better binding affinity with (−7.99 kcal/mol) than Chloroquine (−6.91 kcal/mol). Remdesivir have more a number of residues closer to the ligand anchored in the active site than Chloroquine, showing that Remdesivir is a potent therapeutic inhibitor against 2019-nCoV than chloroquine.

4. Conclusions

We performed molecular docking to assess whether or not it binds to the target with a high affinity for the SARS-CoV-2 protein. According to our results, we noticed that the Parthenolide 5 binds with high affinity to the selected target of the viral protein. We suggest that this compound could be a potential drug for SARS-CoV-2. The Parthenolide 5 compound required further cell validation and could be a hope for the development of anti-SARS-CoV-2 therapy. We also performed molecular docking to study parthenolide 2 and parthenolide 3 against the human liver cancer cell line HEP-G2, our results show that parthenolide 2 has the ability to form a conventional hydrogen bond which has a great importance in the stability of the protein-ligand complex with better binding affinity than standard drugs.

The epoxidation reaction of parthenolide **1** has been investigated using DFT through density functional theory calculations at B3LYP/6–311 G (d,p) computation level. The chemoisomeric reaction pathways associated with this epoxidation have been characterized and explored [57].

Analysis of the CDFT indices accounts for the reactivity of parthenolide **1** was classified as a strong nucleophile and a marginal electrophile. Analysis of the nucleophilic P_k^- Parr functions indicated that the endocyclic (C_3=C_4) double bond of parthenolide **1** is more nucleophilic than exocyclic double bond (C_1=C_1). This characteristic explicated for the chemoselectivity and asynchronicity attained in the C-O bond creation at the most favourable TSs associated with the epoxidation reaction, in addition, analysis of the Gibbs free energy profiles demonstrated that this reaction presented a high chemoselectivity. This epoxidation was taken place through a one-step mechanism, in which the formation of the two new *C-O* single bonds was somewhat asynchronous. The ELF study of the bonding changes along the most favourable reaction path associated with the epoxidation of parthenolide **1**, showed that this reaction initiated with the break of the labile *O-O* single bond of peracetic and with the depopulation of the double bonds of parthenolide **1**. The ensuing break of the *O-H* single bond at the released hydroxyl framework generated anionic oxygen which attacks asynchronously the C3 and C4 carbons of the double bond of parthenolide **1**, producing the formation of the epoxide **P-1**.

Declaration of Competing Interest

No.

CRediT authorship contribution statement

Abdelhak Ouled Aitouna: Investigation, Methodology. **ME. Belghiti:** Data curation, Resources. **Aslı Eşme:** Investigation. **A. Zer-**

oual: Data curation, Formal analysis, Investigation, Resources, Writing - original draft, Writing - review & editing. **M. Salah:** Investigation, Supervision. **A. Chekroun:** Conceptualization. **H. El Alaoui El Abdallaoui:** Funding acquisition. **A. Benharref:** Conceptualization, Supervision. **N. Mazoir:** Formal analysis, Writing - original draft.

Acknowledgments

This research was supported by the MENFPESRS-DESRS, CNRST and UCD.

Supplementary materials

Supplementary material associated with this article can be found, in the online version, at doi:10.1016/j.molstruc.2021.130705.

References

[1] L. Suleimanov, C. Thieuleux, Chapter 19 -well-defined nanoparticles for model studies in sustainable industrial chemistry, Stud. Surf. Sci. Catal. 178 (2019) 399–416.
[2] N. Mazoir, A. Benharref, L. Vaca, M. Reina, A. González-Coloma, Optimization of insecticidal triterpene derivatives by biomimetic oxidations with hydrogen peroxide and iodosobenzene catalysed by Mn^{III} and Fe^{III} porphyrin complexes, Chem. Biodivers. 17 (2020) e2000287.
[3] D. Mansuy, A brief history of the contribution of metalloporphyrin models to cytochrome P450 chemistry and oxidation catalysis, C. R. Chim. 10 (2007) 392–413.
[4] H. El jamili, A. Auhmani, M. Dakir, E. Lassaba, A. Benharref, M. Pierrot, A. Chiaroni, C. Riche, Oxydation et addition des dihalocarbènes sur le β-himachalène, Tetrahedron Lett. 43 (2002) 6645–6648.
[5] N. Mazoir, M. Giorgi, A. Benharref, (4S,5S,10S,13R,14R,17R)-8α,9α-Epoxy-4α,14α-dimethyl-5α-cholestan-3-one, Acta Cryst. E 61 (2005) o3709–o3711.
[6] H. Lu, X. Peter Zhang, Catalytic C-H functionalization by metalloporphyrins: recent developments and future directions, Chem. Soc. Rev. 40 (2011) 1899–1909.
[7] V. Mirkhani, M. Moghadam, S. Tangestaninejad, B. Bahramian, Silica-bound imidazole as a heterogeneous axial ligand for Mn(salophen)Cl: efficient, recoverable and recyclable catalyst for epoxidation of alkenes and hydroxylation of alkanes with sodium periodate, Appl. Catal. A Gen. 313 (2006) 122–129.
[8] N. Mazoir, A. Benharref, L. Vaca, M. Reina, A. González-Coloma, Optimization of insecticidal triterpene derivatives by biomimetic oxidations with hydrogen peroxide and iodosobenzene catalysed by Mn^{III} and Fe^{III} porphyrin complexes, Chem. Biodivers. 17 (2020) e2000287.
[9] M. Daoubi, N. Marquez, N. Mazoir, A. Benharref, R.H. Galán, E. Muñoz, I.G. Collado, Isolation of new phenylacetylingol derivatives that reactivate HIV-1 latency and a novel spirotriterpenoid from Euphorbia officinarum latex, Bioorg. Med. Chem. 15 (2007) 4577–4584.
[10] G. Sudhakar, K. Satish, Nazarov cyclization of divinyl and arylvinyl epoxides: application in the synthesis of resveratrol-based natural products, Chem. Eur. J. 21 (2015) 1–7.
[11] A.A. Abdel Aziz, Synthesis, spectroscopic characterization, thermal studies, catalytic epoxidation and biological activity of chromium and molybdenum hexacarbonyl bound to a novel N_2O_2 schiff base, J. Mol. Struct. 979 (2010) 77–85.
[12] Z. Liu, L. Ma, G.B. Zhou, The main anticancer bullets of the chinese medicinal herb, thunder god vine, Molecules 16 (2011) 5283.
[13] A. Lewinska, P. Chochrek, K. Smolag, E. Rawska, M. Wnuk, Oxidant-based anticancer activity of a novel synthetic analogue of capsaicin, capsaicin epoxide, Redox Rep. 20 (2015) 116.
[14] K.A. Jørgensen, Transition-metal-catalyzed epoxidations, Chem. Rev. 89 (1989) 431–458.
[15] N. Prileschajew, Oxydation ungesättigter verbindungen mittels organischer superoxyde, Ber. der. Dtsch. Chem. Ges. 42 (1909) 4811–4815.
[16] J.L. Bicas, A.P. Dionísio, G.M. Pastore, Bio-oxidation of terpenes: an approach for the flavor industry, Chem. Rev. 109 (2009) 4518–4531.
[17] K.K. Aggarwal, S.P.S. Khanuja, A. Ahmad, T.R. Santha Kumar, V.K. Gupta, S. Kumar, Antimicrobial activity profiles of the two enantiomers of limonene and carvone isolated from the oils of mentha spicata and anethum sowa, Flavour. Fragr. J. 17 (2002) 59–63.
[18] R. Paduch, M. Kandefer–Szerszeń, M. Trytek, J. Fiedurek, Terpenes: substances useful in human healthcare, Arch Immunol. Ther. Exp. 55 (2007) 315–327.
[19] G.I.K. Marei, M.A. Abdel Rasoul, S.A.M. Abdelgaleil, Comparative antifungal activities and biochemical effects of monoterpenes on plant pathogenic fungi, Pestic. Biochem. Physiol. 103 (2012) 56–61.
[20] L.D. Martino, E. Mancini, L.F. Rolim de Almeida, V.D. Feo, The antigerminative activity of twenty-seven monoterpenes, Molecules 15 (2010) 6630–6637.
[21] M. Elmastas, I. Dermirtas, O. Isildak, Antioxidant activity of S-carvone isolated from spearmint (mentha spicata L. Fam Lamiaceae), J. Liq. Chromatogr. Relat. Technol. 29 (2006) 1465–1475.
[22] T.M. Meulemans, G.A. Stork, F.Z. Macaev, B.J.M Jansen, A.D. Groot, Total synthesis of dihydroclerodin from (R)-(−)-carvone, J. Org. Chem. 64 (1999) 9178–9188.
[23] I. Garcia-Bosch, X. Ribas, M. Costas, A broad substrate-scope method for fast, efficient and selective hydrogen peroxide-epoxidation, Adv. Synth. Catal. 351 (2008) 348–352.
[24] D. Sureshkumar, S. Maity, S. Chandrasekaran, Regio- and stereoselective synthesis of aziridino epoxides from cyclic dienes, J. Org. Chem. 71 (2006) 1653–1657.
[25] G. Majetich, R. Hicks, G.R. Sun, M. Gill P, Carbodiimide-promoted olefin epoxidation with aqueous hydrogen peroxide, J. Org. Chem. 63 (1998) 2564–2573.
[26] A. Zeroual, M. Ríos-Gutiérrez, M. El Idrissi, H. El Alaoui El Abdallaoui, L.R. Domingo, An MEDT study of the mechanism and selectivities of the [3+2] cycloaddition reaction of tomentosin with benzonitrile oxide, Int. J. Q. Chem. 119 (2019) e25980.
[27] A. Zeroual, M. Ríos-Gutiérrez, M. Salah, H. El Alaoui El Abdallaoui, R. Domingo L, An investigation of the molecular mechanism, chemoselectivity and regioselectivity of cycloaddition reaction between acetonitrile N-Oxide and 2,5-dimethyl-2H-[1,2,3]diazaphosphole: a MEDT study, J. Chem. Sci. 131 (2019) 75.
[28] A. Zeroual, M. Ríos-Gutiérrez, M. El Ghozlani, M. El Idrissi, A. Ouled Aitouna, M. Salah, El Alaoui, H. El Abdallaoui, L.R. Domingo, A molecular electron density theory investigation of the molecular mechanism, regioselectivity, stereoselectivity and chemoselectivity of cycloaddition reaction between acetonitrile N-oxide and 2,5-dimethyl-2H-[1,2,3]diazarsole, Theor. Chem. Acc. 139 (2020) 37.
[29] L.R. Domingo, M. Ríos-Gutiérrez, P. Pérez, A molecular electron density theory study of the participation of tetrazines in aza-diels-alder reactions, Org. Biomol. Chem. 10 (2020) 15394–15405.
[30] L.R. Domingo, Molecular electron density theory: a modern view of reactivity in organic chemistry, Molecules 21 (10) (2016) 1319.
[31] A. Zeroual, M. Ríos-Gutiérrez, O. Amiri, M. El Idrissi, L.R. Domingo, A molecular electron density theory study of the mechanism, chemo- and stereoselectivity of the epoxidation reaction of R-carvone with peracetic acid, RSC Adv. 9 (2019) 28500–28509.
[32] J. Jeevanandam, K. Pal, M. K.Danquah, Virus-like nanoparticles as a novel delivery tool in gene therapy, Biochimie 157 (2019) 38–47.
[33] A.A. AAljabali, B. Al-Trad, L. AlGazo, G. Alomari, MAl Zoubi, W. Alshaer, K. Al–Batayneh, B. Kanan, K. Pal, M. M.Tambuwala, Gold nanoparticles ameliorate diabetic cardiomyopathy in streptozotocin-induced diabetic rats, J. Mol. Struct. 1231 (2021) 130009.
[34] V. Raji, K. Pal, T. Zaheer, N. Kalarikkal, S. Thomas, F.G. Souza, S.I. Asiya, Gold nanoparticles against respiratory diseases: oncogenic and viral pathogens review, Ther. Deliv. 11 (8) (2020) 521–534.
[35] A. Rabi, K. Pal, S. Fakhar, A. Rahdar, M. Bilal, G. Shahnaz, GZ. Kyzas, A review of the nanomaterials use for the diagnosis and therapy of salmonella typhi, J. Mol. Struct. 1230 (2021) 129928.
[36] D. Kaushik, R. Bhandari, A. Kuhad, TLR4 as a therapeutic target for respiratory and neurological complications of SARS-CoV-2, Exp. Opin. Ther. Targ. (2021), doi:10.1080/14728222.2021.1918103.
[37] P. Singh, K. Pal, A. Chakravraty, Saiqal kram, execution and viable applications of face shield “a safeguard” against viral infections of cross-protection studies: a comprehensive review, J. Mol. Struct. 1238 (2021) 130443.
[38] Y. Ding, Q. Xue, S. Liu, K. Hu, Da Wang, T. Wang, Ye Li, H. Guo, X. Hao, W. Ge, Y. Zhang, A. Li, J. Li, Y. Chen, Q. Zhang, Identification of parthenolide dimers as activators of pyruvate kinase M2 in xenografts of glioblastoma multiforme *in vivo*, J. Med. Chem. 63 (4) (2020) 1597–1611.
[39] SM. O'Donovan, A. Imami, H. Eby, ND. Henkel, J.F. Creeden, X.Z. SophieAsah, R.A. XiaojunWu, J.R. R.TravisTaylor, B.S.4. AlexanderThorman, J. Meller, RE. McCullumsmith, Identifcation of candidate repurposable drugs to combat COVID–19 using a signature–based approach, Sci. Rep. 11 (2021) 4495.
[40] B.O. Villoutreix, R. Krishnamoorthy, R. Tamouza, M. Leboyer, P. Beaune, Chemoinformatic analysis of psychotropic and antihistaminic drugs in the light of experimental anti-SARS-CoV-2 activities, Adv. Appl. Bioinform. Chem. 14 (2021) 71–85.
[41] N. Samad, T.E. Sodunke, A.R. Abubakar, I. Jahan, P. Sharma, S. Islam, S. Dutta, M. Haque, The implications of zinc therapy in combating the COVID-19 global pandemic, J. Inflamm. Res. 14 (2021) 527–550.
[42] M. Moumou, A. El Bouakher, H. Allouchi, A. El Hakmaoui, A. Benharref, V. Mathieu, G. Guillaumet, M. Akssira, Synthesis and biological evaluation of 9α- and 9β-hydroxyamino-parthenolides as novel anticancer agents, Bioorg. Med. Chem. Lett. 24 (2014) 4014–4018.
[43] C. Lee, W. Yang, R.G. Parr, Development of the colle-salvetti correlation-energy formula into a functional of the electron density, Phys. Rev. B 37 (1988) 785–789.
[44] A.D. Becke, Density-functional thermochemistry. III. The role of exact exchange, J. Chem. Phys. 98 (1993) 5648–5652.
[45] W.J. Hehre, L. Radom, P.V.R. Schleyer, J.A. Pople, Ab Initio Molecular Orbital Theory, Wiley, New York, 1986.
[46] H.B. Schlegel, Optimization of equilibrium geometries and transition structures, J. Comput. Chem. 2 (1982) 214–218.
[47] H.B. Schlegel, Modern Electronic Structure Theory, World Scientific Publishing, Singapore, 1994 D. R Yarkony, Ed..
[48] K. Fukui, Formulation of the reaction coordinate, J. Phys. Chem. 74 (1970) 4161–4163.
[49] C. González, H.B. Schlegel, Reaction path following in mass-weighted internal coordinates, J Phys Chem 94 (1990) 5523–5527.
[50] C. González, H.B. Schlegel, Improved algorithms for reaction path following: higher-order implicit algorithm, J. Chem. Phys. 95 (1991) 5853–5860.

[51] J. Tomasi, M. Persico, Molecular interactions in solution: an overview of methods based on continuous distributions of the solvent, Chem. Rev. 94 (1994) 2027–2094.
[52] M. Cossi, V. Barone, R. Cammi, J. Tomasi, Ab initio study of solvated molecules: a new implementation of the polarizable continuum model, Chem. Phys. Lett. 255 (1996) 327–335.
[53] E. Cances, B. Mennucci, J. Tomasi, A new integral equation formalism for the polarizable continuum model: theoretical background and applications to isotropic and anisotropic dielectrics, J. Chem. Phys. 107 (1997) 3032–3042.
[54] V. Barone, M. Cossi, J. Tomasi, Geometry optimization of molecular structures in solution by the polarizable continuum model, J. Comput. Chem. 19 (1998) 404–417.
[55] R.G. Parr, W. Yang, Density Functional Theory of Atoms and Molecules, Oxford University Press, New York, NY, USA, 1989.
[56] L.R. Domingo, P. Pérez, J.A. Sáez, Understanding the local reactivity in polar organic reactions through electrophilic and nucleophilic parr functions, RSC Adv. 3 (2013) 1486–1494.
[57] A. Barhoumi, ME. Belghiti*, M. El Idrissi, A. Zeroual, Physics and Chemistry of Liquids (2020) https://doi.org/10.1080/00319104.2020.1863401.
[58] S. Noury, X. Krokidis, F. Fuster, B. Silvi, Computational tools for the electron localization function topological analysis, Comput. Chem. 23 (1999) 597–604.
[59] M. Salah, A. Zeroual, S. Jorio, H. El Hadki, O. Kabbaj, K. Marakchi, N. Komiha, Theoretical study of the 1,3-DC reaction between fluorinated alkynes and azides: reactivity indices, transition structures, IGM and ELF analysis, J. Mol. Gr. Model. 94 (2020) 107458.
[60] L.R. Domingo, M. Ríos-Gutiérrez, P. Pérez, Applications of the conceptual density functional theory indices to organic chemistry reactivity, Molecules 21 (2016) 748.
[61] A. Zeroual, A. Benharref, A. El Hajbi, Theoretical study of stereoselectivity of the [1 + 2] cycloaddition reaction between (1S,3R,8S)-2,2-dichloro-3,7,7,10-tetramethyltricyclo[6,4,0,01.3]dodec-9-ene and dibromocarbene using density functional theory (DFT) B3LYP/6-31G*(d), J. Mol. Model. 21 (2015) 44.
[62] A. El Haib, R. El ajlaoui, M. El Idrissi, M. Moumou, S. Abouricha, A. Zeroual, A. Benharref, A. El Hajbi, The mechanism, the chemoselectivity and the regioselectivity of the 1-benzyl-4-ethynyl-1H-[1,2,3]triazole and 1-azidomethyl-4-tert-butyl-benzene in [3+2] cycloaddition reactions: a DFT study, Mor. J. Chem. 6 (2018) 14–21.
[63] A. Zeroual, A. El Hajbi, Understanding the regioselective and molecular mechanism of the TCE in cycloaddtion reaction (TCE+Cp) and addition reaction (TCE+HCl) using DFT calculation, Can. Chem. Trans. 3 (2015) 430–437.
[64] M.J. Turner, J.J. McKinnon, S.K. Wolff, D.J. Grimwood, P.R. Spackman, D. Jayatilaka, M.A. Spackman, Crystal Explorer, University of Western Australia, 2017.
[65] R.M. Wiedhopf, M. Young, E. Bianchi, J.R. Cole, Tumor Inhibitory Agent from Magnolia grandiflora (Magnoliaceae) I: parthenolide, J Pharm Sci 62 (1973) 345.
[66] Z. Liu, S. Liu, Z. Xie, R.E. Pavlovicz, J. Wu, P. Chem, J. Aimiuwu, J. Pang, D. Bhasin, P. Neviani, J.R. Fuchs, C. Plass, P.K. Li, C. Li, T.H.M. Huang, L.C. Wu, L. Rush, H. Wang, D. Perrotti, G. Marcucci, K.K. Chan, Modulation of DNA methylation by a sesquiterpene lactone parthenolide, J. Pharmacol. Exp. Ther. 329 (2009) 505–514.
[67] G.M. Morris, R. Huey, W. Lindstrom, M.F. Sanner, R.K. Belew, D.S. Goodsell, A.J. Olson, AutoDock4 and autodocktools4: automated docking with selective receptor flexibility, J. Comput. Chem. 30 (2009) 2785–2791.
[68] M.F. Sanner, Python: a programming language for software integration and development, J. Mol. Gr. Mod. 17 (1999) 57.
[69] Z. Jin, X. Du, Y. Xu, Y. Deng, M. Liu, Y. Zhao, B. Zhang, X. Li, L. Zhang, C. Peng, Y. Duan, J. Yu, L. Wang, K. Yang, F. Liu, R. Jiang, X. Yang, T. You, X. Liu, X. Yang, F. Bai, H. Liu, X. Liu, L.W. Guddat, W. Xu, G. Xiao, C. Qin, Z. Shi, H. Jiang, Z. Rao, H. Yang, Structure of mprofrom SARS-CoV-2 and discovery of its inhibitors, Nature 582 (2020) 289–293.
[70] M.M. Othman I, M. Gad-Elkareem MA, E. Anouar, M. Snoussi, K. Aouadi, A. Kadri, Novel fused pyridine derivatives containing pyrimidine moiety as prospective tyrosyl-tRNA synthetase inhibitors: design, synthesis, pharmacokinetics and molecular docking studies, J. Mol. Struct. 1219 (2020) 128651.